Rock and Soil Mechanics

Volume 42 | Issue 10 Article 7

1-12-2022

Analysis of wave-type and seismic component induced by rock blasting considering source characteristics

Qi-dong GAO
School of Highway, Chang'an University, Xi'an, Shaanxi 710064, China

Wen-bo LU
Key Laboratory of Rock Mechanics in Hydraulic Structural Engineering of the Ministry of Education, Wuhan University, Wuhan, Hubei 430072, China

Zhen-dong LENG
China Gezhouba Group Explosive Co., Ltd., Chongqing 401121, China, zdleng@whu.edu.cn

Ya-qiong WANG
School of Highway, Chang'an University, Xi'an, Shaanxi 710064, China

See next page for additional authors

Custom Citation

GAO Qi-dong, LU Wen-bo, LENG Zhen-dong, WANG Ya-qiong, ZHOU Hai-xiao, ZHANG Shi-chao, . Analysis of wave-type and seismic component induced by rock blasting considering source characteristics[J]. Rock and Soil Mechanics, 2021, 42(10): 2830-2844.

Analysis of wave-type and seismic component induced by rock blasting considering source characteristics

Authors

Qi-dong GAO, Wen-bo LU, Zhen-dong LENG, Ya-qiong WANG, Hai-xiao ZHOU, and Shi-chao ZHANG

Rock and Soil Mechanics 2021 42(10): 2830−2844 ISSN 1000−7598
https: //doi.org/10.16285/j.rsm.2021.5108 rocksoilmech.researchcommons.org/journal

Analysis of wave-type and seismic component induced by rock blasting considering source characteristics

GAO Qi-dong[1], LU Wen-bo[2], LENG Zhen-dong[3], WANG Ya-qiong[1], ZHOU Hai-xiao[1], ZHANG Shi-chao[1]

1. School of Highway, Chang'an University, Xi'an, Shaanxi 710064, China
2. Key Laboratory of Rock Mechanics in Hydraulic Structural Engineering of the Ministry of Education, Wuhan University, Wuhan, Hubei 430072, China
3. China Gezhouba Group Explosive Co., Ltd., Chongqing 401121, China

Abstract: The blasting induced seismic waves are generally composed of compressional wave (P-wave), shear wave (S-wave), and Rayleigh wave (R-wave), however, wave-type and seismic components are not differentiated in the attenuation law and safety criteria for the current blast vibration studies. In this study, a method of wave-type discrimination is used for the seismic wave prediction based on polarization direction. Using theoretical analysis and numerical modelling, the blasting source characteristics and the radiated wave-types are investigated for different shapes of explosive charge. Combined the results of the site blasting experiments, the wave-type and seismic components induced by three typical blast-holes are analyzed and three blast holes include the single vertical blast-hole, the smooth blast-hole, and the slope pre-splitting blast-hole. The source characteristics and acting mechanism are then discussed for different blast-holes. The dominant wave-type at special location is predicted for three blast types. The research results indicate that the blasting source of the vertical blast-hole can be viewed as a delay superposition of the short explosive column. All the P-, S-, and R-waves contribute to the ground surface vibration from the vertical blast-hole. With the increase of the blasting-target distance, it is found that the S-wave gradually deviates from its dominant radiation direction, while the P-wave mainly contributes to the horizontal radial vibration, and the R-wave dominates the vertical vibration. Because the horizontal smooth blast-hole and the slope pre-splitting blast-hole are both contour blast-holes, the two blast holes have a similar acting mechanism, in which the main acting force is the loading from the normal surface. The S- and R-waves are the dominant seismic wave types within the blasting contour surface, whereas the role of the P-wave is negligible. Besides, the R-wave becomes the dominant wave-type as the blasting center distance increases; however, the contribution of P-wave outside the contour surface cannot be ignored.

Keywords: rock blasting; blasting-induced seismic wave; source characteristics; wave-type and seismic components; dominant wave-type

1 Introduction

Rock blasting excavation or mining has been widely used in important infrastructure fields such as the mining industry, water conservancy, transportation, and municipal. When explosives blast in the rock and soil medium, beyond the engineering purposes such as rock breaking, some portion of the blasting energy is converted into blasting seismic waves. Once the blasting vibration reaches a certain intensity, it will not only endanger the safety of the project itself, but also cause vibration damage to the surrounding buildings (structures), facilities, and equipment[1−2]. In this consideration, the safety evaluation and control of blasting vibration have been a key concern in the field of rock blasting[3−5].

As for blast vibration study, three parameters are normally used to describe, they are amplitude, frequency, and duration[1]. The prediction and control of blast vibration are therefore basically based on the research of the three parameters. Due to the good correlation between the peak particle velocity (PPV) and the structure damage[6], PPV is often used as an index to measure and evaluate the safety of blast vibration. A large number of researches have emerged on the study of PPV attenuation law and its prediction equation. The empirical prediction equations were represented by the Sachs' cube root equation[7] and the square root equation of the U.S. Bureau of Mines[8]. The soft-computing approach was developed premised on modern computer technology such as artificial neural networks[9−10], gray-scale correlation analysis[11], and genetic algorithms[12] for forecasting. Moreover, because the building (structure) damage extent is closely related to the frequency f, many studies have been conducted on the attenuation rule of dominant frequency and the prediction aspects[13−14].

Received: 15 January 2021 Revised: 6 July 2021
This work was supported by the National Natural Science Foundation of China (52009003, 51809016), the Fundamental Research Funds for the Central Universities (300102210123) and the Open Research Funds of Key Laboratory of Rock Mechanics in Hydraulic Structural Engineering Ministry of Education (EMHSE1903).
First Author: GAO Qi-dong, male, born in 1991, PhD, Lecturer, mainly engaged in teaching and research in the field of engineering blasting and rock dynamics. E-mail: qdgao@chd.edu.cn
Corresponding author: LENG Zhen-dong, male, born in 1989, PhD, Senior Engineer, mainly engaged in research on rock dynamics and engineering blasting, E-mail: zdleng@whu.edu.cn

At present, the frequency-dependent (PPV-*f*) safety criterion has been accepted and widely used internationally.

It has been shown that surface blasting ground motion usually results from a combined action of the compressional (P), shear (S), and Rayleigh surface (R) waves[15], as shown in Fig. 1. Due to the differences in wave propagation velocity, polarization characteristics, and attenuation, the evolution of wave components and dominant wave pattern will be expected. Existing studies of the blast vibration attenuation laws and safety criteria, however, do not honor the differences between the wave type and component, changing of the dominant wave pattern will inevitably lead to various response patterns or damage types to the target structure. It is of great importance to analyze the wave components and patterns of the rock blasting induced seismic waves.

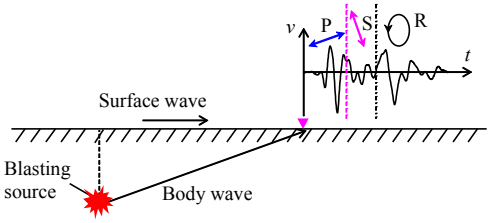

Fig. 1 Wave-types and seismic components of ground blasting

In addition, the actual borehole blasting will involve different types of blast-holes such as main blast-hole (BH) or buffering BH, smooth blast-hole and pre-splitting BH. For a dam foundation excavation, as depicted in Fig. 2, different typical BHs can be found. These BHs have obvious differences in many aspects such as charging structure, detonation mode, and layout orientation of BHs. These differences will lead to various blasting source characteristics, and the interaction mechanism between the blast source, explosive load and rock mass is not the same, which will inevitably cause differences in the wave types and components of the blasting seismic waves[16−17]. Referring to the features and action mechanism of blasting seismic wave, many researches have been conducted on the analysis of stress wave fields induced by different charging shapes. Favreau[18], Graff[19], and Achenbach[20] analyzed the stress wave field radiated by a spherical charge using a spherical cavity model, and they stated that only uniform P wave was induced and radiated. Heelan[21] derived an analytical displacement solution of a short column explosive based on a short column cavity model, the results showed that the short column charge can produce both the P and SV waves, and both waves have a specific dominant radiation orientation. Considered the blasting velocity and the charge length and based on Heelan's short column solution, Blair[22] derived a computational model for extended charge superposition, and explored the Mach effect of the P- and SV-waves.

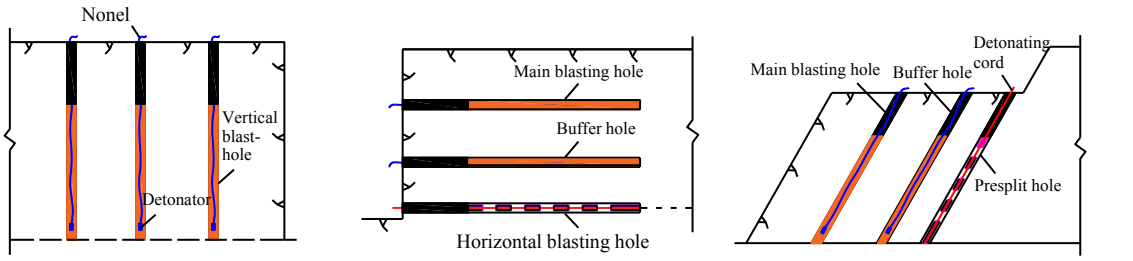

(a) Vertical hole bench blasting (b) Slope presplitting blasting (c) Horizontal smooth blasting of protective layer

Fig. 2 Different typical blasting holes in dam foundation excavation

Considering the differences in the source characteristics and the evolution of blast-induced wave-types and seismic components in the actual blasting, a wave-type identification method is adopted in this study based on a prediction approach of the polarization direction. In addition, the blasting source characteristics of different charge shapes and the radiated wave-types are investigated through a combination of theoretical analysis and numerical modelling. Based on the measured vibration waveforms and certain typical blast-holes in rock blasting, the wave-type and seismic components induced by different kinds of blast-holes were further studied, and the acting mechanism is also discussed. The research results can enrich the research content of rock blasting seismic effect and can provide a reference for blasting vibration safety evaluation and control considering various wave patterns.

2 Classification and wave-type identification of rock blasting seismic wave

2.1 Classification and characteristics of blast-induced seismic wave

When the explosion happens in the rock and soil media, beyond the engineering purposes such as rock fragmentation, some portion of the blasting energy may also cause disturbance to the surrounding rock and soil mass. This disturbance will transfer from one site to the other site and from near field to far field, which is then propagated as the form of blasting seismic wave. For the first time, Poisson and Stokes[23] discovered

and proved that in an infinite and homogeneous elastic medium, two independent elastic waves are propagated, namely the longitudinal and transverse waves, and the propagation velocity satisfies:

$$\left.\begin{aligned} C_{\mathrm{P}} &= \sqrt{\frac{\lambda+2\mu}{\rho}} \\ C_{\mathrm{S}} &= \sqrt{\frac{\mu}{\rho}} \end{aligned}\right\} \tag{1}$$

where C_{p} and C_{s} are the propagation velocities of the longitudinal and transverse waves; ρ is the medium density; λ and μ are the Larmé constants. The movement direction of the P wave is the same as the wave propagation direction. For the P wave, only a volume deformation without rotational deformation exists. The P wave is also called the expansion wave or compression wave. While for the S wave, the movement direction is perpendicular to the wave propagation direction, only a rotational deformation exists without volume deformation. The S wave is also known as rotational wave or shear wave. Because the P wave travels faster than that of the S wave, the P wave is normally observed firstly and then followed by the S wave. The two waves are also known as the P wave (primary wave) and the S wave (secondary wave). The S wave can be subdivided into SH and SV components based on the different mass movement directions. Because the P and S waves only propagate within the medium and do not show boundary effect, the P and S waves are also regarded as body waves.

Body waves only exist in the infinite and homogeneous media, but when a body wave reaches a free surface, another class of waves that propagates along the free surface is formed, namely, surface waves. Rayleigh first discovered and proved the existence of surface waves, and the surface waves thus named as Rayleigh waves (Rayleigh waves, or R-wave for short). The R wave is confined and propagated to the ground surface of the media, and displacement decay exponentially along with the depth. Additionally, there is a π/2 difference in phase between the horizontal and vertical displacements, and its particle trajectory shows a counterclockwise elliptical shape at the free surface[24]. The propagation velocity of R-wave is slightly smaller than that of S-wave, which can be approximately estimated by[20]:

$$C_{\mathrm{R}} \approx \frac{0.862+1.14\nu}{1+\nu} C_{\mathrm{S}} \tag{2}$$

where C_{R} denotes the propagation velocity of R-wave; ν is Poisson's ratio. In addition to Rayleigh waves, there are other types of surface wave such as Stoneley wave and Love wave. Stoneley wave refers to a generalized Rayleigh wave, which is characterized as a non-uniform wave that exists at the interfaces of different media and propagates along the interfaces; while Love wave is formed by the mutual interference of S-wave between the upper soft and lower hard media layers, which belongs to SH-type waves.

Due to the expansion loading of explosive being normally symmetric, and the SH wave is not co-plane with the P and the SV waves, the SH component of the S wave is usually negligible in the blast[25]. In this consideration, this study is mainly focused on the analysis of three waves, the P, SV, and R waves. Figure 3 shows the propagation and motion characteristics of the three waves[26].

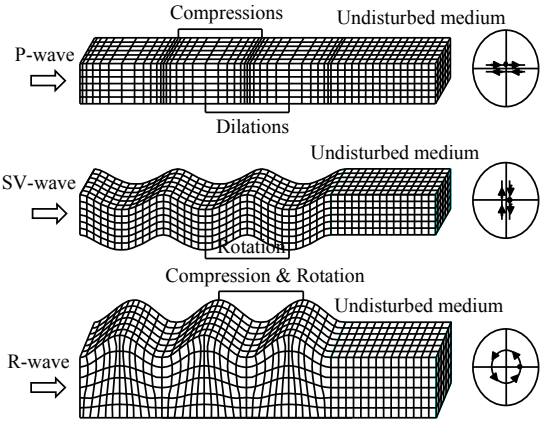

Fig. 3 Propagation and motion characteristics of different seismic waves[26]

2.2 Wave-type identification based on polarization direction prediction

As mentioned above, propagation velocity and polarization direction are the two main differences for different types of waves, and a variety of methods for seismic phase identification and wavefield separation have been derived in the field of seismology. The methods can be broadly classified into two categories: the kinematics (apparent velocity) method[27] and the dynamics (polarization properties) method[28−29]. Many methods in seismology, however, require a large amount of computational processing of the original data, and the wave propagation path is very complex and unclear. Compared the rock blasting with natural earthquakes, the boundary conditions of blasting are much simpler, and its source mechanism and wave propagation path are relatively known. Because of these, the prediction of different wave propagation paths and polarization directions can be realized. Based on the idea of polarization filtering in seismology, Gao et al.[16−17] proposed an identification method of blast-induced seismic components based on the prediction of the polarization direction.

2.2.1 Polarization direction prediction

Prior to analysis of the wave-type of blasting seismic

waves, the polarization direction of various wave types can be predicted based on the relative position of the source and the measurement target point, including three scenarios: (a) the measurement point is located on top of the blasting (seismic) source elevation, namely the upstream wave and the P-wave is then polarized in the 1st and 3rd quadrants, and the horizontal and vertical vibrations are in the same phase (the phase difference is zero); while the S-wave is polarized in the 2nd and 4th quadrants, and the horizontal and vertical vibrations are just in the opposite phases (the phase difference is π); (b) the measurement point is located underneath the blasting (seismic) source elevation, that is, the downgoing wave, the P wave is polarized in the 2nd and 4th quadrants, the horizontal and vertical vibrations are just in the opposite phases with a phase difference of π, while the S wave is polarized in the 1st and 3rd quadrants, the horizontal and vertical vibrations have the same phase with phase difference of 0; and (c) the measurement point and the blasting (seismic) source have the same elevation, under this case, the P/S wave is mainly polarized in the horizontal/vertical direction. Moreover, under the above three cases, the R wave is polarized elliptically and a counterclockwise ellipse is observed for the particle motion trajectory on the ground surface. The phase difference is π/2 between the horizontal and vertical vibration. The upgoing wave is taken as an example to show the polarization direction and phase difference of the three seismic waves, as presented in Fig. 4.

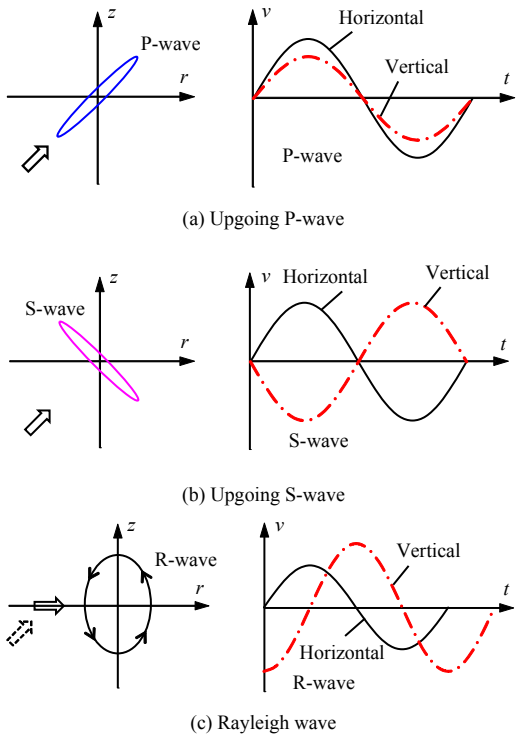

Fig. 4 Polarization direction and phase difference of the upstream wave

2.2.2 Wave-type identification method

As mentioned in the last Section and to sum, on the one hand, the wave-types and seismic components of the blasting seismic wave can be identified by analyzing the characteristics of the particle motion trajectory, i.e., vector analysis of particle motion diagram; on the other hand, the arrival time of different waves can also be identified by comparing the phase difference between the horizontal and vertical vibrations, i.e., phase difference analysis of blasting vibration. Due to the variation of polarization direction and propagation velocity of different seismic waves, the shape of the particle motion trajectory and the phase difference of vibration waveform may change with the arrival of different wave types. In addition, because the particle trajectories are also plotted by time sequence point, there should be a one-to-one correspondence in the time domain between the inflection points in the particle trajectories (represents the arrival time of different waves) and the change points of the phase difference in the waveforms. In this way, it can be then verified against each other and details about the verification procedure can be found in the references[16−17].

3 Blasting source characteristics and induced wave types of different explosive charge shapes

3.1 Mechanics simplification of the explosive charge with different shapes

3.1.1 Mechanical simplification of spherical charge

For the blasting of a spherical charge in an infinite homogeneous rock mass, in general, it can be considered as the mechanical issue of a spherical cavity subjected to a dynamic internal pressure (as shown in Fig.5)[19]. Under the action of uniform internal pressure in a spherical cavity, only radial displacement is hence produced in the rock mass, and the circumferential (tangential) displacement is zero. Only a radially expansion wave (P-wave) is formed during the blasting of a spherical charge, and the disturbance will spread outward as a spherical wave.

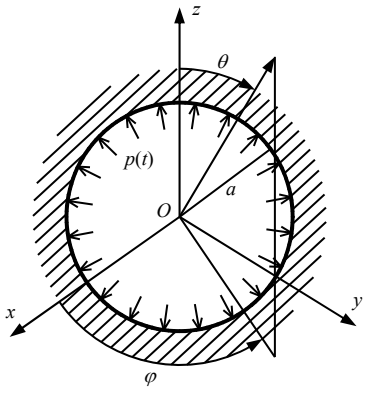

Fig. 5 Simplified mechanical model of the spherical charge[19]

3.1.2 Mechanics simplification of short column charge

Unlike the spherical charge, the blasting stress wave field of columnar charge is not uniformly radiated. In addition to the P-wave, a significant S-wave is also excited. Heelan[21] assumed the blasting of a short columnar charge can be considered to be a short column cavity that is subjected to radial internal pressure problem, and derived a displacement solution for the mechanical problem. The results show that both P- and SV waves associate with a specific dominant radiation orientation (as shown in Fig. 6).

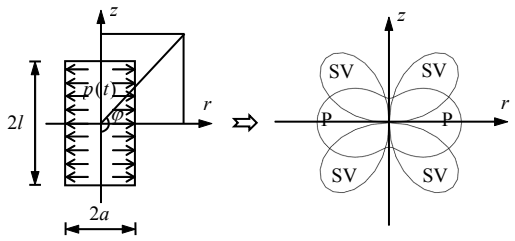

Fig. 6 Simplified mechanical model of the short explosive column and its source radiation pattern[21]

3.1.3 Mechanical simplification of extended charge

As for the extended charge, Blair et al.[22] studied the displacement solution based on the solution of Heelan's short column. If the long column charge is decomposed into *n* short column units, as shown in Fig.7, and then overlay along the axial direction of the charge according to the explosive blast velocity, the solution of the extended charge can be obtained. Based on the results of Blair et al.[22], it is found that under certain conditions, the radiated stress waves by each short column unit may interfere with each other and thus form a conical Mach wave (see Fig. 7). In Fig.7, PL and SL stand for the loading terms of P- and S-waves, respectively; while PU and SU denote the unloading terms of P- and S-waves, respectively, and the waves radiate outward in the form of spherical waves, but the loading and unloading terms are generally weak if the conical wave is formed.

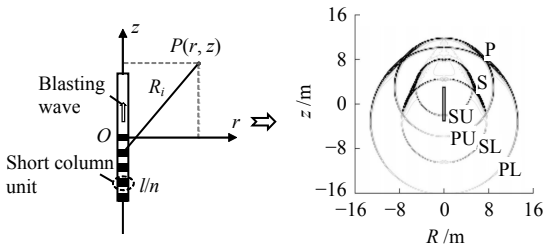

Fig. 7 Computation model of the stress wave field of the extended charge and its displacement contour[22]

3.2 Numerical modelling of blasting of different shapes of explosive charge

3.2.1 Numerical models and parameters

Numerical simulation is conducted to further study the wave patterns of seismic wave radiated by spherical and column charges. Based on the symmetry of the problem, as shown in Fig. 8, two cases of 1/4 model are built. Case 1 is an infinite rock mass model (without considering free surface) and the model dimension is 100 m×100 m × 100 m (length × width × height), which contains 763,203 zones and 735,048 nodes. To eliminate the influence of reflected waves at the model boundaries, non-reflecting bounders are applied to all model boundaries except the symmetric boundary. Case 2 is a semi-infinite rock mass model (considering a free surface) and its size is 100 m×100 m× 55 m (length×width×height), which contains 515,053 zones and 492,953 nodes. In the modelling, the dosage of the two charge types is the same, the diameter of the spherical charge is 0.42 m, and the diameter of the column charge is 90 mm, and the length is 6.0 m. There is a 5.0 m distance between the free surface and the center of both the spherical and the column charge.

The JWL state equation is used to model the gas pressure during the explosive detonation process:

$$P = A\left(1-\frac{\omega}{R_1 V}\right)\mathrm{e}^{-R_1 V} + B\left(1-\frac{\omega}{R_2 V}\right)\mathrm{e}^{-R_2 V} + \frac{\omega E_0}{V} \quad (3)$$

where P is the detonation pressure; V is the relative volume of the detonation products; E_0 is the initial specific internal energy; A, B, R_1, R_2 and ω are the parameters related to the explosive types. In the modelling, #2 rock emulsion explosive is used and its parameters are shown in Table 1. The ALE grid is employed for the explosive and the Lagrange grid is used for the rock mass, and the load transfer between the two grids is realized by the flow−solid coupling algorithm.

A homogeneous elastoplastic constitutive model is chosen for the rock mass, which can simplify the boundary conditions and eliminate the interference of complex factors, although the discontinuous mechanical behavior of the rockmass is ignored to a certain extent in the near blast area. In this way, it can be analyzed clearly for the stress wave patterns and types radiated by different charge shapes. The physical deformation and mechanical parameters of the rock mass are shown in Table 2.

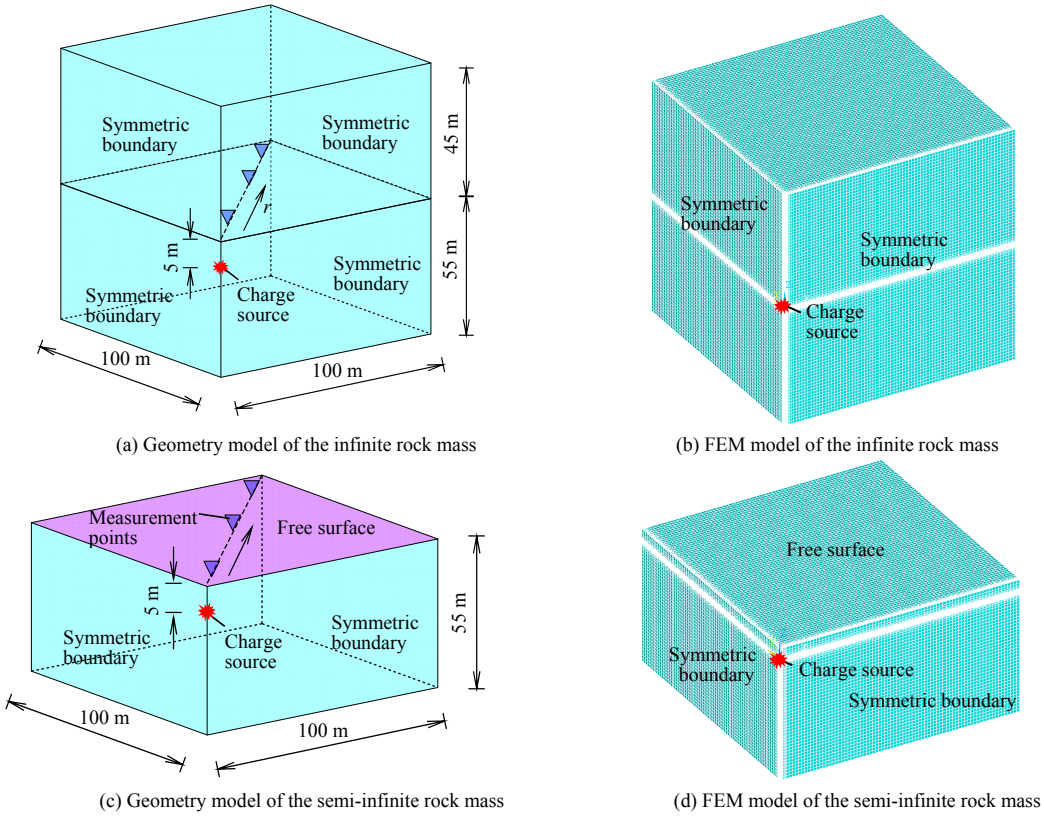

(a) Geometry model of the infinite rock mass

(b) FEM model of the infinite rock mass

(c) Geometry model of the semi-infinite rock mass

(d) FEM model of the semi-infinite rock mass

Fig. 8 Numerical models of the spherical and cylindrical charges

Table 1 JWL parameters of #2 rock emulsion

Density /(kg • m^{-3})	Detonation velocity /(m • s^{-1})	P /GPa	A /GPa	B /GPa	R_1	R_2	ω
1 000	4 000	3.24	220	0.2	4.5	1.1	0.35

Table 2 Physical and mechanical parameters of rock mass

Density /(kg • m^{-3})	Dynamic elastic modulus /GPa	Poisson's ratio	Yield strength /MPa	Hardening index
2 700	25	0.25	20	0.3

3.2.2 Modelling results of spherical charge

Figure 9 shows the stress contour of a spherical charge blasting in an infinite rock mass, it is seen that the stress wave field radiated from the spherical charge is dispersive outward uniformly, in other words, the detonation of the spherical charge excites only the expansion wave (P-wave). Figure 10 shows the blast vibration waveforms and particle motion vectors at a measurement point during the blasting in the infinite rock mass and semi-infinite rock mass. For the measurement points in the infinite rock mass, it is seen from Fig. 10 that the blast vibration waveform shows a neat and smooth shape, which can be considered as a gradually decaying sine wave. The wave mainly contains one radiation source and the vector diagram of the particle motion only contains the upstream wave that polarized along with the 1st and 3rd quadrants, which is the P-wave. This observation indicates that the blasting of the spherical charge only excites the P-wave in the infinite rock mass. While for the measurement point in the semi-infinite rock mass, the blast vibration waveform is not a simple decaying sinusoidal P-wave; another radiation source is found after the P-wave propagation. The particle firstly shows a linear polarization in 1st and 3rd quadrants, and then converts into a counterclockwise elliptical motion, which actually belongs to the R-wave motion.

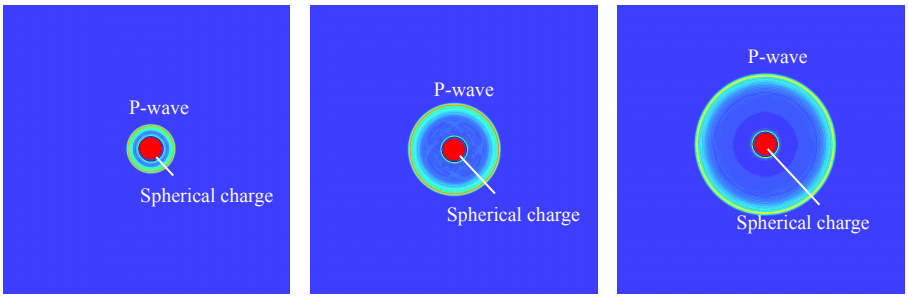

(a) t =115 μs (b) t =230 μs (c) t =360 μs

Fig. 9 Stress contours of the spherical charge in infinite rock mass

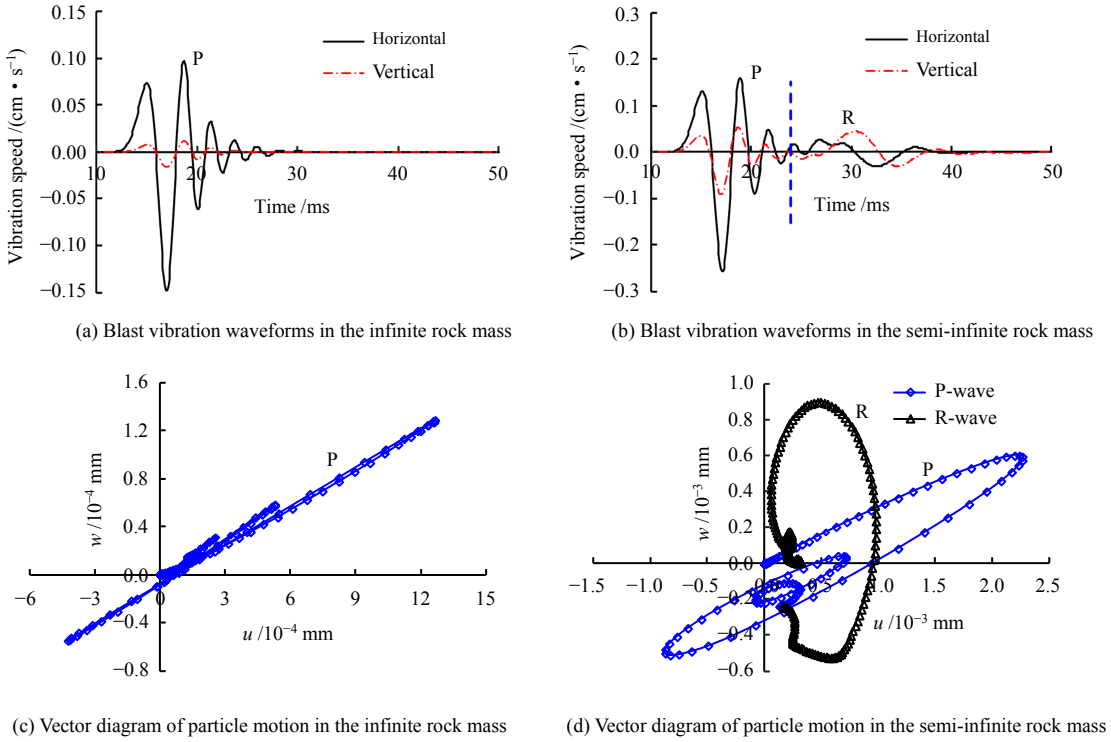

(a) Blast vibration waveforms in the infinite rock mass

(b) Blast vibration waveforms in the semi-infinite rock mass

(c) Vector diagram of particle motion in the infinite rock mass

(d) Vector diagram of particle motion in the semi-infinite rock mass

Fig. 10 Analysis of wave-type and seismic component caused by the spherical charge

3.2.3 Modelling results of cylindrical charge

By varying the inputs of rock mass or explosive blast, the blasting stress contours of the columnar charge are obtained under different detonation conditions, as shown in Fig.11. It is seen that the stress wave field morphology varies largely that radiated by the columnar charge under different detonation conditions. Regardless of the case, both P- and S-waves are produced for the columnar charge. Whether the cone Mach wave is formed is closely related to the relative magnitude of the explosive velocity of detonation (VOD) and the rock acoustic velocity (C_P)[22].

Using the input parameters of the rock mass and explosive parameters described above (the supersonic case, VOD>C_P), the blast vibration waveforms and particle motion vectors at a measurement point during the blasting are shown in Fig. 12. It is seen that for the measurement points in the infinite rock model, both the blast vibration waveform and the vector diagram of the particle motion contain two induction sources, the P-wave and S-wave that radiated by the column charge, respectively. The P-wave is still polarized along with the 1st and 3rd quadrants, while the motion of the S-wave is relatively weak at the two measurement points. As for the measurement points in the semi-infinite rock mass model, the blast vibration also contains the R-wave motion beyond the P-wave and S-wave. Since the wave velocities of the R-wave and S-wave are relatively close to each other, some portion of S-wave is covered by the later arriving R-wave. Because the various waves are not sufficiently separated clearly in the time domain and the overlap is found with each other, it should be noted that the letters P, S, or R labeled in the figure only represent strictly the dominant wave type of the corresponding time period and this assumption holds true for the rest of the text.

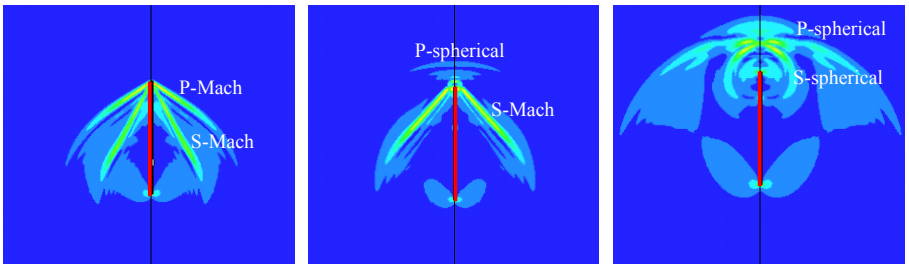

(a) VOD> C_P (b) C_S<VOD<C_P (c) VOD<C_S

Fig. 11 Stress contours of the cylindrical charge under different detonation conditions

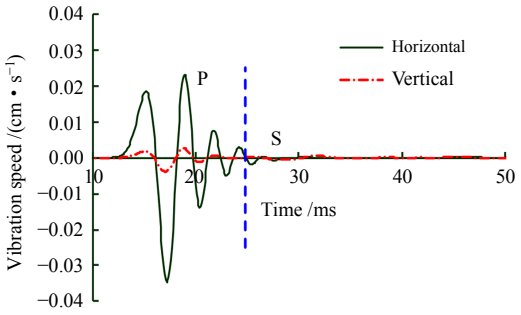

(a) Blast vibration waveforms in the infinite rock mass

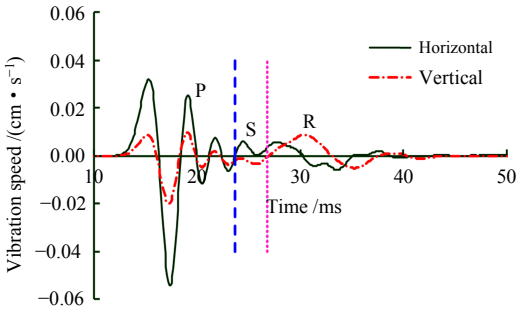

(b) Blast vibration waveforms in the semi-infinite rock mass

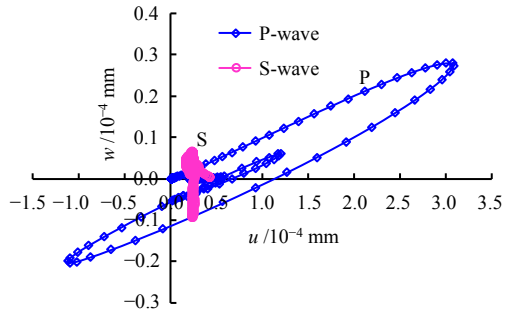

(b) Vector diagram of particle motion in the infinite rock mass

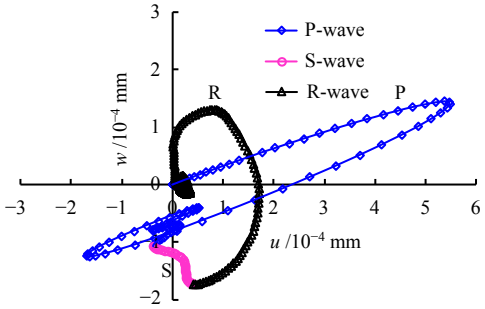

(b) Vector diagram of particle motion in the semi-infinite rock mass

Fig. 12 Analysis of the wave-type and seismic components caused by the cylindrical charge

4 Field tests of seismic waves induced by different kinds of typical blast-holes

To further study the differences in wave-types and seismic components induced by different kinds of blasting source, combined with a hydropower station rock foundation blasting excavation, several field blasting tests or excavation blasting vibration monitoring data are selected in order to analyze the wave-types and seismic components induced by three typical blast-holes, including the vertical single holes, the horizontal smooth blasting holes and the slope pre-splitting blasting holes.

4.1 Vertical single holes

4.1.1 Blasting design and measurement point layout

Figure 13 shows a photo of the field test for the vertical hole blasting test. Four vertical blast-holes are drilled at the four corners of a square with 3.5 m×3.5 m. These four blast-holes are detonated within the same blasting network (Fig.14(a)), and in-hole delay detonators are used to separate blast vibration waveforms from each blast-hole. The name of the detonator segment and delay times for the four blast- hole are marked as A, B, C, D, and MS1 (0 ms), MS5 (110 ms), MS9 (310 ms), and MS13 (650 ms), respectively. Table 3 and Fig. 15 give detail information on the borehole charging parameters and charging structure. The detonators of A and B holes are placed in the upper part (upper detonation), while the detonators of C and D holes are placed in the lower part (bottom detonation), which are not included in this study.

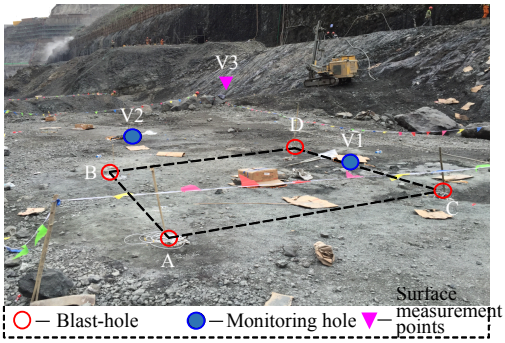

Fig. 13 Layout of blast-holes in the vertical-hole field blasting experiment

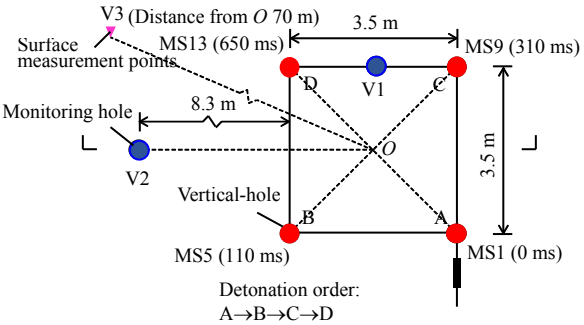

(a) Plane view of the vertical-hole and measurement point layout

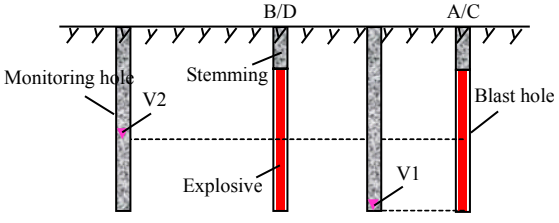

(b) Cross section view of the vertical-hole

Fig. 14 Layout of blast-holes in the vertical-hole field blasting experiment

Table 3 Drilling and blasting parameters in the vertical-hole blasting experiment

B.H. diameter /mm	B.H. depth /m	B.H. spacing /m	Charge diameter /m	Charge length /m	Charge weight /kg	Stemming length /m
100	6	3.5	32	4.5	4.5	1.5

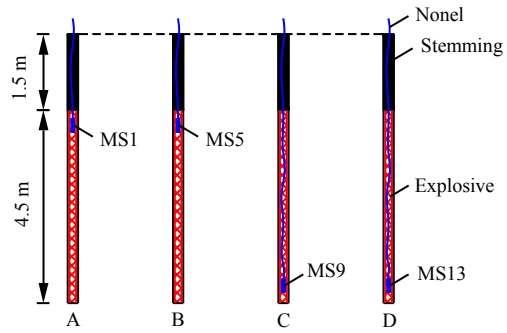

Fig. 15 Charging structures in the vertical-hole blasting experiment

To monitor the blasting vibration within the rock mass and on the ground surface, two in-hole measurement points and one surface measurement point are arranged in the test (as shown in Fig. 13 and Fig. 14(b)), where the V1 monitoring hole is located in the center of the CD line and the elevation is the same with the elevation of the blast hole bottom. The V2 monitoring hole is located 8.3 m away from the BD line and the elevation of the measurement point is the same as the elevation of the charge middle section. The #3 surface measurement point is 70 m away from the center of the four blast holes. A set of the uni-axial sensor, including both the horizontal and vertical directions, is placed at each in-hole measurement point for the V1 and V2 holes, and a tri-axial sensor is placed at the V3 surface monitoring point. TC-4850 blast vibration test system, produced by Chengdu Zhongke Measurement and Control Co., Ltd, is used for the field test. The sampling frequency of the data logger is 8 000 s^{-1}, the triggering value is set as 0.25 cm/s, the recording duration is 5.0 s, and the pre-trigger is set as 0.1-0.2 s. The tri-axial vibration sensor is a set of TC-4850 logger system and with a measurement capacity of 35 cm/s. The uni-axial vibration sensor is a model of CDJ28 with a measurement capacity of 200 cm/s. This test system is also used for the other two field tests in the following sections.

Figure 16 shows the measured typical blast vibration time−history (at the V2 point), which contains the vibration waveforms induced by the four blast holes. Because the blast vibrations are separated sufficiently and the distances among holes are large enough for each blast hole, the blasting of the four holes can be considered as single-hole blasting. For ease of description, V1-A is used to represent the blast vibration at the V1 point induced by hole A.

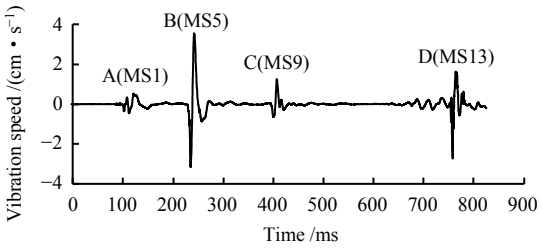

Fig. 16 Measured blast vibration time−history in the vertical-hole blasting experiment (V2)

4.1.2 Experiment results

(1) Blasting seismic waves within the rock mass

Figure 17 shows the typical vector diagrams of particle motion and blast vibration waveforms at V1 and V2 points within the rock mass. Because the V1 point is located below the center elevation of the charge (downgoing wave), the P-wave is polarized along with the 2nd and 4th quadrants. The phases are just opposite for the horizontal and vertical vibration. The S-wave is polarized along with the 1st and 3rd quadrants and the phase of the horizontal and vertical vibration is the same. In addition, the V2 measurement point is at the same elevation as the charge center. The P-wave mainly moves along the horizontal direction, while the S-wave mainly propagates along the vertical direction. It is seen that the vibration at V1 and V2 measurement points is mainly contributed from the P and S waves, and little contribution from the R waves. Because the V1 and V2 monitoring points are located within the rock mass, vibration is mainly caused by the body wave. The R waves are not fully developed because it is mainly formed on the ground free surface and due to the short distance between the two points and the blasting sources.

(2) Blasting seismic waves at free surface

Figure 18 shows the vector diagram of the particle motion and the blast vibration waveform at the surface monitoring point (V3 point). Because the V3 point is placed above the center elevation of the charge (upgoing wave), the P-wave is polarized along with the 1st and 3rd quadrants, and the phases of the horizontal and vertical vibration are the same, while the S-wave is polarized along with the 2nd and 4th quadrants, and the horizontal and vertical vibration have opposite phases. It is seen that the surface blast vibration contains the contributions from the P-wave, S-wave, and R-wave during the vertical hole blasting, however, the S-wave motion is relatively weak at this point, and it mainly shows the motion of P-wave and R-wave.

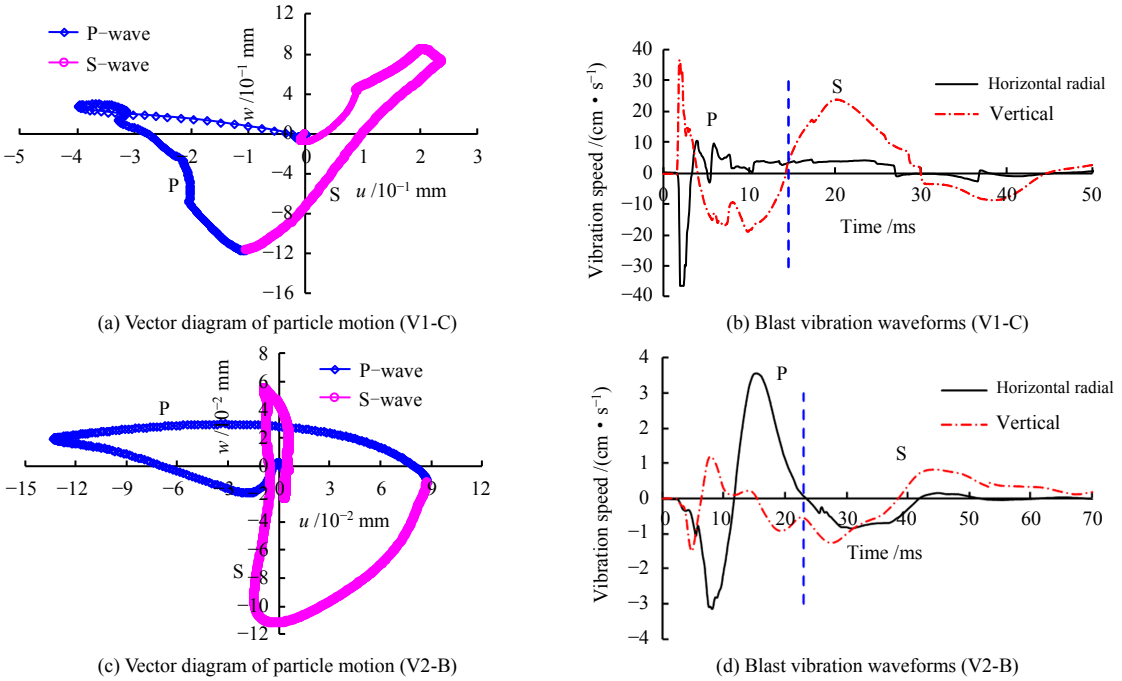

(a) Vector diagram of particle motion (V1-C)

(b) Blast vibration waveforms (V1-C)

(c) Vector diagram of particle motion (V2-B)

(d) Blast vibration waveforms (V2-B)

Fig. 17 Analysis of the blast-induced wave-type and seismic component within the rock mass

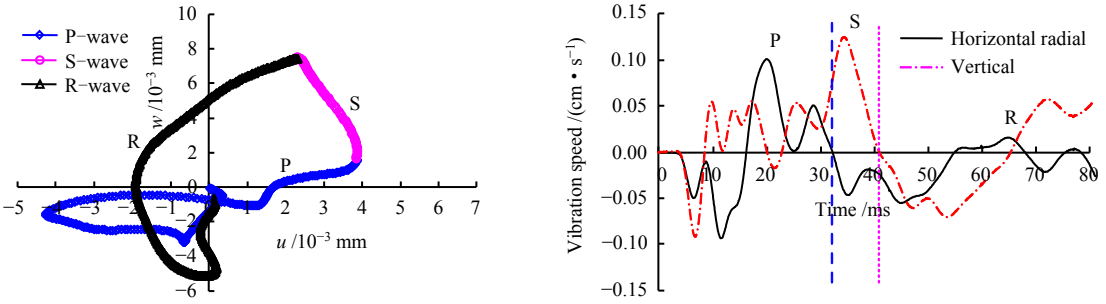

(a) Vector diagram of particle motion (V3-A)

(b) Blast vibration waveforms (V3-A)

Fig. 18 Analysis of the blast-induced wave-type and seismic components at the ground surface

4.2 Horizontal smooth blasting holes

4.2.1 Layout of blast-holes and monitoring points

Figure 19 shows a photo of the horizontal smooth blasting holes field experiment. Totally, four surface monitoring points (S1−S4) are arranged in the plane with the same height of the smooth blasting holes (S1−S3), and 3.5 m above the smooth blasting holes (S4). Figure 20 shows a cross-cut of the relative location between the measuring points and the blast holes. In the experiment, 32 blast-holes are arranged and these blast holes are divided into eight sections using millisecond delay detonators MS5 (110 ms). For each section, about three to six blast-holes are included. The blast-hole spacing is 0.6 m, the average resistance line is 1 m, and the blast-hole depth is 10 m. The explosive is #2 rock emulsion explosive and an air spacing charge technique is adopted for charging. The charging linear density is 220 g/m, and the detailed drilling and charging parameters are given in Table 4 and a typical blast-hole charging structure is shown in Fig. 21. Figure 22 shows the measured typical blast vibration–time curve (S2 point), which includes eight segments of waveform induced by the smooth blasting.

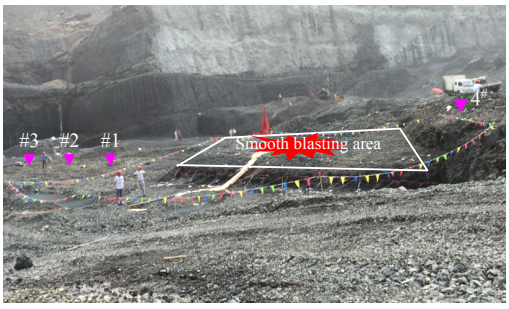

Fig. 19 Layout of blast-holes and monitoring points in the field horizontal smooth blasting experiment

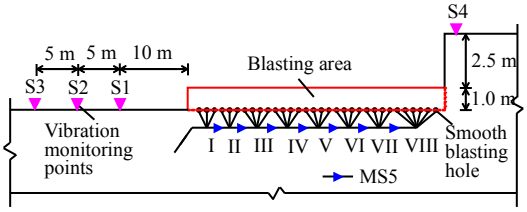

Fig. 20 Location relationship between the blast-holes and monitoring points in the field horizontal smooth blasting experiment

Table 4 Drilling and blasting parameters in the horizontal smooth blasting experiment

B.H. diameter /mm	B.H. depth /m	B.H. spacing /m	Charge diameter /mm	Linear density /(g • m^{-1})	Single hole mass /kg	Clogging length /m
76	10	0.6	32	220	2.2	1

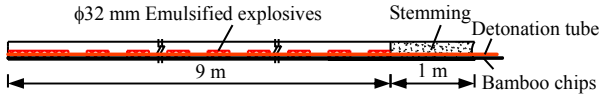

Fig. 21 Typical charging structure in the horizontal smooth blasting experiment

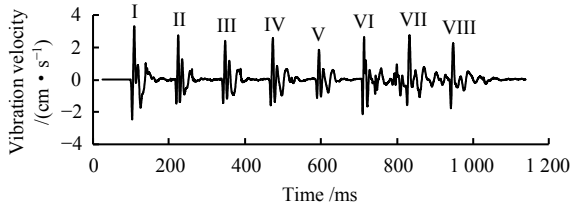

Fig. 22 Measured blast vibration time−history in the horizontal smooth blasting experiment (S2)

For ease of description, S1-I represents the blast vibration induced by the first section of the smooth blasting at the S1 measurement point.

4.2.2 Experiment results

(1) Blasting seismic waves on the smooth blast hole surface

Figure 23 shows the typical vector diagram of the particle motion and the blast vibration waveforms on the same surface of the smooth blast-holes. As the measurement points #1−#3 are at the same elevation with the blast-holes (parallel waves), the P-wave is mainly polarized horizontally, while the S-wave is mainly polarized in the vertical direction, and the R-wave is polarized in a counterclockwise elliptical. For the measurement points on the same surface with the blast-holes, it is seen that the P-wave can barely be identified and its contribution can be ignored, but clear motion characteristics is observed for the S-wave and R-wave. This indicates that both the S-wave and R-wave are important components, and the S-wave is mainly propagated in the vertical direction, while the R-wave has a contribution to both the horizontal and vertical vibration components. It should be noted that the vertical dashed line in Fig.23(b) roughly represents the dividing point between the S-wave and R-wave motions, and the dividing point coincides well with the time when the inflection point appears in the vector diagram of particle motion (Fig. 23(a)). Since the wave velocity difference is small between the S and R waves, the S wave portion contains part of the R wave at the initial arrival stage, and the R wave also contains the tail portion of the S wave. In light of this, the marks only represent the dominant wave type of the corresponding propagation period. In addition, for the S1-VII point, it is seen from Fig.23(b) that the vibration velocity of the horizontal S-wave is much lower than that of the R-wave, but the vibration velocity of the vertical S-wave is comparable to that of the R-wave. This observation indicates that the horizontal vibration at this point is mainly caused by the R-wave, while the vertical vibration results from both the S-wave and R-wave.

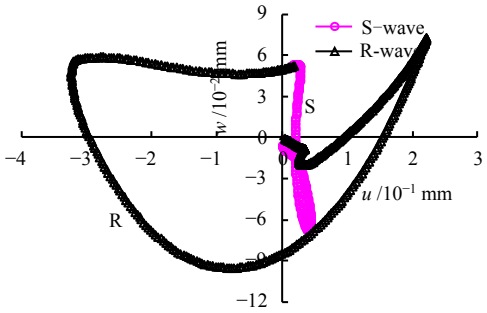

(a) Vector diagram of particle motion (S1-VII)

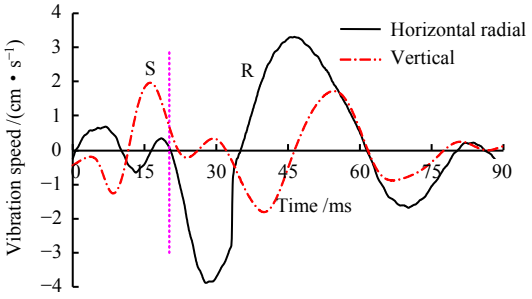

(b) Blast vibration waveforms (S1-VII)

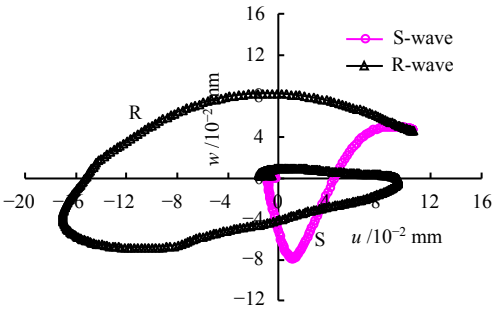

(c) Vector diagram of particle motion (S2-I)

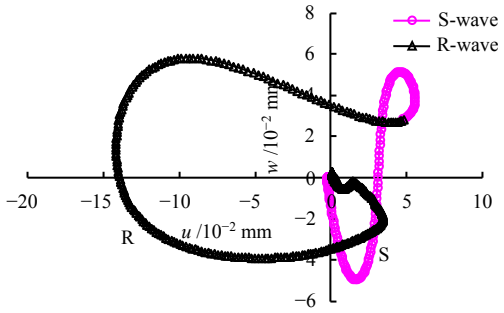

(d) Vector diagram of particle motion (S3-I)

Fig. 23 Analysis of the blast-induced wave-type and seismic component on the same surface of smooth blast-holes

(2) Blasting seismic waves outside the smooth blast-hole surface

Figure 24 shows the typical vector diagram of the particle motion and the blast vibration waveforms of monitoring points located beyond the surface of smooth blast holes. Because the S4 location is 3.5 m higher than the blast-hole (upgoing wave), the P wave mainly propagates along the direction of the 1st and 3rd quadrants, while the S-wave mainly moves along the direction of the 2nd and 4th quadrants, and the R-wave still shows a counterclockwise elliptical motion. For the points outside the surface of the blast-holes, the motions of the P wave, S wave, and R wave are observed clearly, and the role of P-wave cannot be ignored under such a case. In addition, Fig. 24(b) also shows that the vibration velocity of the P-wave at #4-II is significantly higher than that of the other two waves, while the vibration velocities of the S and R waves are comparable. This observation indicates that the P wave is the dominant wave type at S4-II among the three wave types.

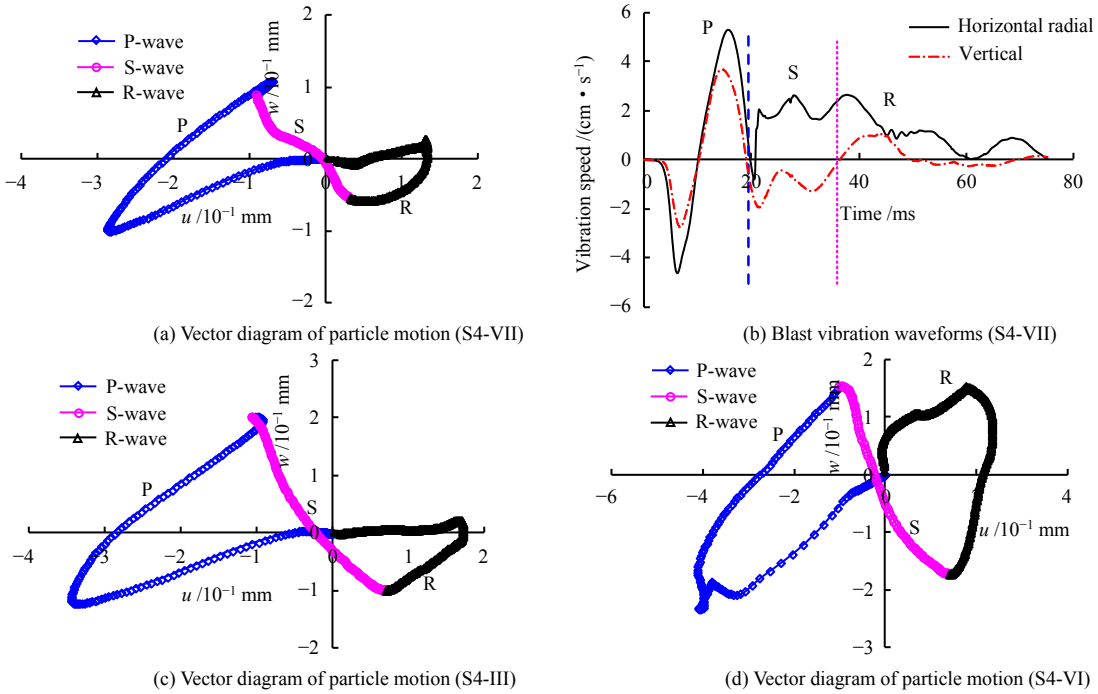

(a) Vector diagram of particle motion (S4-VII)

(b) Blast vibration waveforms (S4-VII)

(c) Vector diagram of particle motion (S4-III)

(d) Vector diagram of particle motion (S4-VI)

Fig. 24 Analysis of the blast-induced wave-type and seismic component outside the surface of smooth blast-holes

4.3 Slope pre-splitting blasting holes

4.3.1 Layout of monitoring points for the pre-splitting blasting

Combined with a gentle section excavation of a hydropower dam foundation, field testing of slope pre-splitting blasting was conducted. In the field test, three surface blasting vibration monitoring points (P1 to P3) were placed along with the formed slope profile, and the measurement points were about 10 m to 13 m away from the top surface of the pre-splitting holes, as shown in Fig. 25. Figure 26 shows the section view of the blast-holes and monitoring points. Figure 27 gives the blasting initiation network in the slope pre-splitting blasting test. The blast test contains one row of pre-splitting holes, three rows of main blast holes, and one row of buffer holes. Millisecond detonator MS5 (110 ms) is used for the time delay between the rows. The 3−4 of the pre-splitting holes are the first blasting ring, and the segment is divided into 10 segments using millisecond detonator MS3 (50 ms) for the time delay purpose. The main blast-hole and buffer-hole are designed as a single-hole shot. The millisecond detonator MS13 (650 ms) is used for time delay in boreholes, and the millisecond detonator MS3 (50 ms) delay is also used for the time delay between the different boreholes. For the pre-splitting blast-holes, the drilling and blasting parameters and the charging structure are shown in Table 5 and Fig. 28, respectively. Figure 29 shows a field measured blast vibration time curve (P2 point), which includes ten segments of the pre-splitting hole induced vibration waveforms and several segments of main blast-hole trigged vibration waveforms.

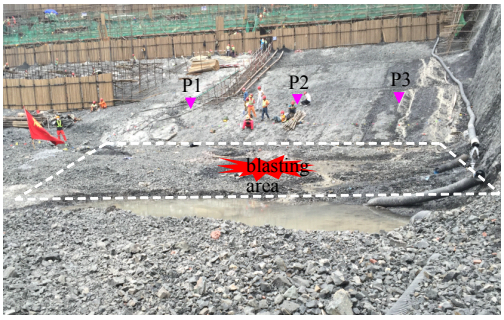

Fig. 25 Layout of monitoring points in the field slope pre-splitting blasting experiment

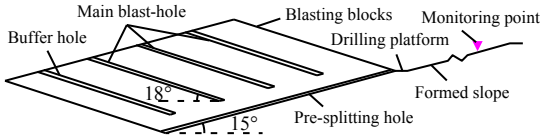

Fig. 26 Cut view of the blast-holes and monitoring points in the slope presplitting blasting experiment

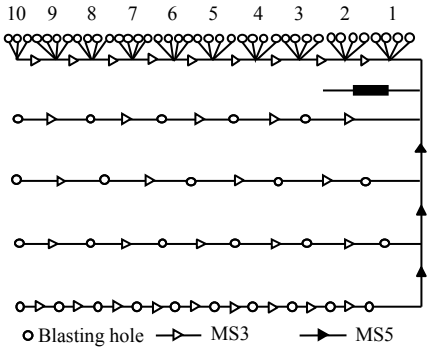

Fig. 27 Blasting initiation network in the slope pre-splitting blasting experiment

Table 5 Drilling and blasting parameters in the slope pre-splitting blasting experiment

B.H. diameter /mm	B.H. depth /m	B.H. spacing /m	Charge diameter /mm	Linear density /(g • m^{-1})	Single hole charge /kg	Clogging length /m
76	10	0.6	32	220	2.2	1

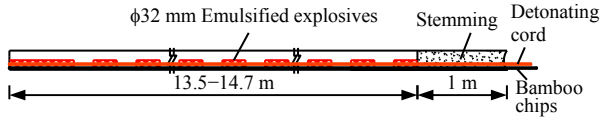

Fig. 28 Typical charging structure in the slope pre-splitting blasting experiment

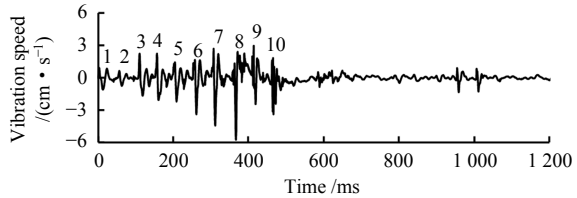

Fig. 29 Measured blast vibration time-history in the slope pre-splitting blasting experiment (P2)

4.3.2 Experiment results

Through extracting a portion of the blast vibration waveforms from the pre-splitting blast-holes, the corresponding particle motion vector and blast seismic waveforms can be obtained, as shown in Fig. 30. Since all the monitoring points are located at the formed slope profile, and the slope profile plane and the plane of the pre-splitting hole (pre-splitting surface) is basically parallel with a very small distance, it is then safe to assume the measurement points are all located on the pre-splitting surface. The orientation of the pre-splitting surface is also marked as a dashed blue line in Fig. 30. If the coordinate system is rotated with the pre-splitting surface as the reference, then the measurement points and the blast sources can be considered to be with the same elevation (parallel wave). It is seen from Fig. 30 that the blasting seismic waves mainly consist of S and R-waves on the pre-splitting surface, and the P-wave is hard to be identified. The S-wave propagates mainly in the direction that is perpendicular to the pre-splitting surface, while the R waves contribute to both the directions that are along and perpendicular to the pre-splitting surface. The R waves show nearly a counterclockwise elliptical trajectory. From the blasting vibration waveforms at the P2 point, it is seen that the peak vibration velocity of the R wave is higher than that of the S-wave, which indicates that R-wave is the dominant wave type herein. Due to the errors of vibration waveform extraction, the skewed sensor arrangement, and the small undulation of the terrain, it is worth to be noted that there should have some extent of distortion for the vector diagram of the particle motion; however, the change of the dominant waveform can be judged based on the inflection point in the vector diagrams.

4.4 Acting mechanism and wave-type prediction of different kinds of blast-holes

To sum, a large difference is found between the wave-types and components of the seismic waves radiated by different blast-holes. In other words, the wave patterns and components of rock blasting seismic waves are closely related to the characteristics of the blast source. The main differences between the three typical blast-holes are the charging structure, detonation mode, and the layout of blasting borehole orientation. Specifically: (1) As for the vertical single-hole blasting, the limited speed of explosive blast needs to be considered with continuously loaded and blasted by the detonator. The source is equivalent to the extended charge described in section 3.1.3, the extended charge calculation model (Fig.7) can be used as a reference for the mechanical simplification of the vertical single-hole blasting (see Fig.31 (a)). (2) As for the horizontal smooth blast-hole, the air spacing technique is used for charging and the explosive is initiated by the detonating cord. The detonation speed of the detonating cord is very fast and the charges can be viewed as simultaneous detonation. The contour blast-holes are normally fired simultaneously. In light of this, the action role of the horizontal smooth blast holes can be simplified to a normal load on the smooth blast surface (Fig.31(b)). Additionally, when considering the mechanical interactions among the blast-holes, a small amount of horizontal load also exists in this condition. (3) As for the slope pre-splitting blast-holes, the charge structure and detonation mode are the same as the smooth blast-holes. The main difference between the two methods is the layout of the blast-hole orientation. Thus, the simplified mechanics model is equivalent to the mechanical model of the horizontal smooth blast-

hole and the mechanics model should be rotated by a certain angle (see Fig.31(c)).

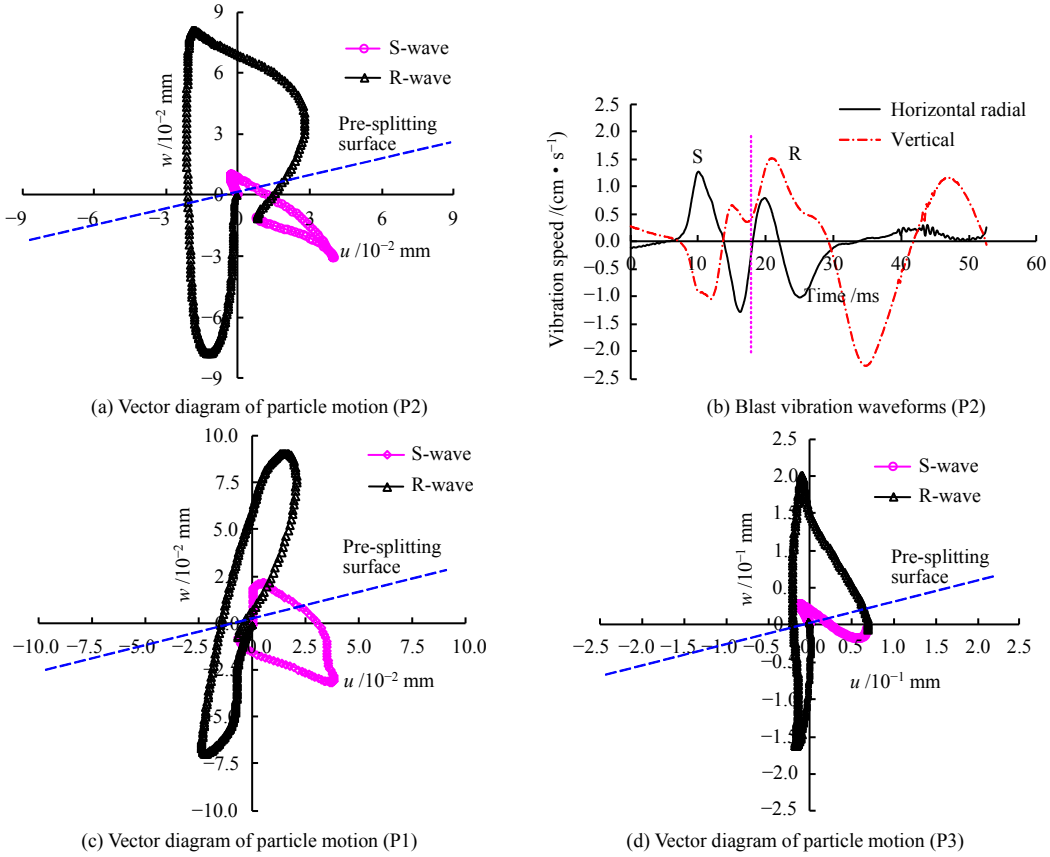

(a) Vector diagram of particle motion (P2)

(b) Blast vibration waveforms (P2)

(c) Vector diagram of particle motion (P1)

(d) Vector diagram of particle motion (P3)

Fig. 30 Analysis of the blast-induced wave-type and seismic component on the pre-splitting surface

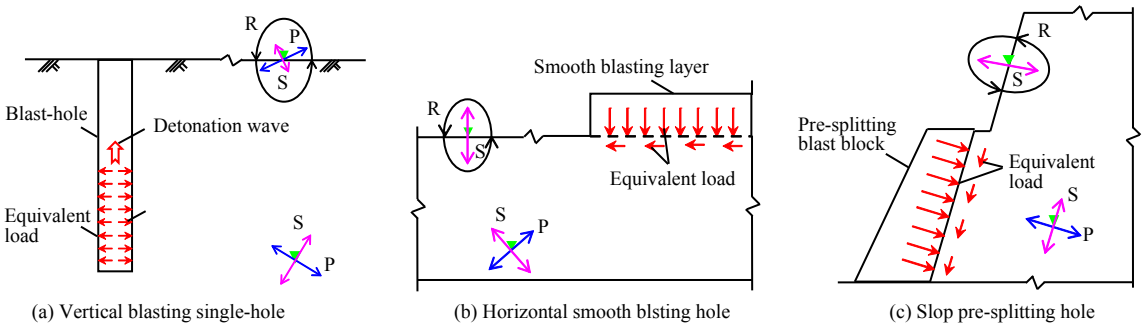

(a) Vertical blasting single-hole

(b) Horizontal smooth blsting hole

(c) Slop pre-splitting hole

Fig. 31 Simplified mechanical model of different types of blast-holes and the wave-type prediction

In addition to the characteristics of the blasting source, the wave type and components of blasting seismic waves are also related to other factors such as spatial location of the monitoring point, different wave propagation and attenuation laws. Through analyzing the acting mechanism of different blast-holes, and combined with the field test results, the blast-induced wave-types can be predicted as follows:

(1) Blast source of the vertical single hole is equivalent to a buried cylindrical charge, which can excite P and S-waves simultaneously (see Figs. 11 and 12). Both the numerical modelling (see Fig.12) and field test measurements (see Fig.18) show that the surface blast vibration contains all the contributions from P, S and R waves. As the blast source–target distance increases, however, the measurement point gradually deviates from the dominant radiation azimuth of the S-wave (i.e., 45°, see Fig. 6), and it then closes to the dominant radiation azimuth of the P-wave (horizontal radial). The S-wave role is hence relatively weak at the ground surface. The P-wave mainly acts on the horizontal radial vibration and because of the slow decay rate of the R-wave, the vibration in the vertical direction will be dominated by the R-wave in the far field[16]. For measurement points within the rock mass, the R-wave effect can be negligible, and the relative weights of the P and S waves are related to the relative location between the measurement point and the blast source (see Fig.17). The wave-type is shown in Fig.31(a) for the vertical hole blasting at a typical location.

(2) The horizontal smooth blast-hole and the slope

pre-splitting hole belong to the profile holes. They have a similar action mechanism, which is dominated by the normal load on the profile surface and it mainly consists of the S and R-waves at the profile surface (see Figs. 23, 30). On the contrary, the motion of the P-wave is relatively weak. Due to the slow decaying of the R-wave, with the increasing of the blast source–target distance, the R-wave will be the dominant wave-type[17]. For the monitoring point outside the profile surface, the motion of the P-wave is not negligible (see Fig.24), while the dominant wave-type is related to the relative location between the measurement point and the blast source. Figures 31(b) and 31 (c) show the wave patterns for the horizontal smooth blast-hole and the slope pre-splitting blast hole, respectively.

5 Conclusions

Considering the differences of blast source characteristics in field blasting, the wave-types and components of rock blasting induced seismic waves are analyzed, and the main conclusions are as follows:

(1) The spherical charge blasting is equivalent to the problem of dynamic internal pressure in a spherical cavity, which mainly excites a uniformly P-wave. The cylindrical charge blasting is similar to a delayed superposition of the dynamic internal pressure of a short columnar cavity, which can simultaneously excite the P and S waves with specific dominant radiation azimuth.

(2) The blasting source of the vertical single hole is equivalent to a buried cylindrical charge, which can simultaneously excite the P and S waves. The surface blast vibration contains the contribution from all the P, S, and R-waves. As the blast source–target distance increases, the S wave deviates gradually from its dominant radiation azimuth. The P wave mainly acts on the horizontal radial vibration, while the R wave will dominate the vertical vibration.

(3) The horizontal smooth blast-hole and the slope pre-splitting hole belong to the profile holes with the same action mechanism. The blasting seismic waves mainly consist of the S and R-waves at the profile surface, while the contribution of the P-wave is relatively weak. As the blast source–target distance increases, the R-wave will become the dominant wave type and the motion of the P-wave cannot be ignored.

It should be mentioned that only three types of typical blast-holes are selected in this study and the differences of seismic wave types and components are analyzed due to different blast source characteristics. Other studies still need to conduct for other different blast-holes and a more effective separation method is worth exploring for wave components for future study for the purpose of studying the propagation and attenuation law of different waves.

References

[1] SINGH P K, ROY M P. Damage to surface structures due to blast vibration[J]. International Journal of Rock Mechanics and Mining Sciences, 2010, 47(6): 949−961.

[2] FAN Yong, LU Wen-bo, ZHOU Yi-hong, et al. A model for predicting vibration peak induced by blasting excavation under high in-situ stress[J]. Rock and Soil Mechanics, 2017, 38(4): 1082−1088.

[3] LU Wen-bo, LI Hai-bo, CHEN Ming, et al. Safety criteria of blasting vibration in hydropower engineering and several key problems in their application[J]. Chinese Journal of Rock Mechanics and Engineering, 2009, 28(8): 1513−1520.

[4] YANG Jian-hua, YAO Chi, LU Wen-bo, et al. Vibration frequency characteristics of surrounding rock of deep tunnel induced by borehole-blasting[J]. Rock and Soil Mechanics, 2017, 38(4): 1195−1202.

[5] LI Xin-ping, BIAN Xing, LUO Yi, et al. Study on attenuation law of blasting vibration propagation of side wall of underground cavern[J]. Rock and Soil Mechanics, 2020, 41(6): 2063−2069.

[6] MCGARR A. Estimating ground motions for small nearby earthquakes[C]//Seismic Design of Embankments and Caverns. New York: ASCE, 1983: 113−127.

[7] LÜ Tao, SHI Yong-qiang, HUANG Cheng, et al. Study on attenuation parameters of blasting vibration by nonlinear regression analysis[J]. Rock and Soil Mechanics, 2007, 28(9): 1871−1878.

[8] LEI Zhen. Research and application on nonlinear prediction methods of bench vibration effect[D]. Beijing: China University of Mining & Technology, 2015.

[9] KHANDELWAL M, SINGH T N. Prediction of blast-induced ground vibration using artificial neural network[J]. International Journal of Rock Mechanics and Mining Sciences, 2009, 46(7): 1214−1222.

[10] LU Xue-dong, FAN Xin-yu, DAI Zhen-wei, et al. BP neural network application and model modification in prediction of open-pit mine blasting vibration parameters[J]. Journal of Central South University (Science and Technology), 2013, 44(12): 5019−5024.

[11] LIU Ya-qun, LI Hai-bo, PEI Qi-tao, et al. Prediction of peak particle velocity induced by underwater blasting based on the combination of grey relational analysis and genetic neural network[J]. Rock and Soil Mechanics, 2013, 34(Suppl.1): 259−264.

[12] DINDARLOO S R. Prediction of blast-induced ground vibrations via genetic programming[J]. International Journal of Mining Science and Technology, 2015, 25(6): 1011−1015.

[13] ZHOU Jun-ru, LU Wen-bo, ZHANG Le, et al. Attenuation of vibration frequency during propagation of blasting seismic wave[J]. Chinese Journal of Rock Mechanics and Engineering, 2014, 33(11): 2171−2178.

[14] LI H, LI X, LI J, et al. Application of coupled analysis methods for prediction of blast-induced dominant vibration frequency[J]. Earthquake Engineering and Engineering Vibration, 2016, 15(1): 153−162.

[15] DOWDING C H. Blast vibration monitoring and control[M]. Englewood Cliffs: Prentice-Hall, Inc., 1985.

[16] GAO Qi-dong, LU Wen-bo, YANG Zhao-wei, et al. Components and evolution laws of seismic waves induced by vertical-hole blasting[J]. Chinese Journal of Rock Mechanics and Engineering, 2019, 38(1): 18−27.

[17] GAO Qi-dong, LU Wen-bo, YANG Zhao-wei, et al. Components and attenuation of seismic waves induced by horizontal smooth blasting[J]. Explosion and Shock Waves, 2019, 39(8): 170−182.

[18] FAVREAU R F. Generation of strain waves in rock by an explosion in a spherical cavity[J]. Journal of Geophysical Research, 1969, 74(17): 4267−4280.

[19] GRAFF K F. Wave motion in elastic solid[M]. Oxford: Clarendon Press, 1975.

[20] ACHENBACH J D. Wave propagation in elastic solids[M]. New York: North-Holland Publishing, 1973.

[21] HEELAN P A. Radiation from a cylindrical source of finite length[J]. Geophysics, 1953, 18(3): 685−696.

[22] BLAIR D P. Seismic radiation from an explosive column[J]. Geophysics, 2010, 75(1): 55−65.

[23] KUZMENKO A A, VOROBEV V D, DENISYUK II, et al. Seismic effects of blasting in rock[M]. [S. l.]: [s. n.], 1993: 16−22.

[24] FOTI S, LAI C, RIX G, et al. Surface wave methods for near-surface characterization[M]. Boca Raton: CRC Press, 2014.

[25] ZHENG Zhi-zhen, ZHU Chuan-zhen, HU Zuo-chun. Differences between explosions and earthquakes[J]. Chinese Journal of Geophysics, 1975, 18(3): 208−216.

[26] KING M. Rock quality, seismic velocity, attenuation and anisotropy[M]. Nick Barton: Taylor and Francis, 2007.

[27] LI Xian, WANG Wen-jie, CHEN Bing-rui. AB algorithm suitable for identifying the microseismic signal and first arrival of P-wave automatically at the project scale[J]. Chinese Journal of Rock Mechanics and Engineering, 2017, 36(3): 681−689.

[28] ZHANG Chu-xuan, LI Xi-bing, DONG Long-jun, et al. A S-wave phase picking method with four indicators of three functions for microseismic signal in mines[J]. Chinese Journal of Rock Mechanics and Engineering, 2015, 34(8): 1650−1659.

[29] YANG Zhao-wei, LU Wen-bo, GAO Qi-dong, et al. An S-wave phase picking method for blasting seismic waves and its application in engineering[J]. Explosion and Shock Waves, 2018, 38(1): 28−36.